Geosciences
Geociências

Structure and tectonic significance of high- and low-temperature deformation along the lateral escape-related Guaçuí and Batatal shear zones, southern Araçuaí Orogen (southeastern Brazil)

http://dx.doi.org/10.1590/0370-44672020730043

Marcos Eduardo Hartwig[1,3]
https://orcid.org/0000-0002-2661-7506
Marilane Gonzaga de Melo[1,4]
https://orcid.org/0000-0003-3397-3258
César Augusto Moreira[2,5]
https://orcid.org/0000-0002-9504-7025

[1]Universidade Federal do Espírito Santo - UFES, Departamento de Geologia,Centro de Ciências, Naturais e da Saúde, Alegre - Espírito Santo – Brasil.

[2]Universidade Estadual Paulista - UNESP, Departamento de Geologia, Instituto de Geociências e Ciências Exatas, Rio Claro - São Paulo - Brasil.

E-mails: [3]marcos.hartwig@ufes.br, [4]marilane.melo@ufes.br, [5]moreirac@rc.unesp.br

Abstract

The Guacuí and Batatal lineaments in the southern region of the state of Espírito Santo (southeastern Brazil) can be traced from satellite images for tens of kilometers. They are considered shear zones associated to the final tectonic stages of the Araçuaí-West Congo (A-WC) Orogen during the Ediacaran-Cambrian period. In order to understand their nature and tectonic implications for the development of the orogeny, we integrated geological and structural data based on fieldwork and detailed microstructural analysis. Data was collected along two profiles located at the central segments of both structures. The results demonstrated that the Guaçuí shear zone (GSZ) is a typical ductile transpressive shear zone with approximately 9 km width that shows numerous dextral kinematic indicators and records metamorphism of upper amphibolite facies. The GSZ shows different levels of intensity of dynamic deformation. The Batatal shear zone (BSZ) is a narrow brittle shear zone that shows essentially brittle microstructures (intercrystalline microfractures) revealing deformation at low-grade conditions (frictional regime). Based on their characteristics and the level of erosion of the rocks exposed in the region, we interpret that GSZ developed prior to BSZ.

Keywords: mylonites, microfractures, deformation, Araçuaí orogen, shear zones.

1. Introduction

Shear zones are linear to curvilinear strips of strained rocks that exist in all scales, whose length is much greater than width. These geological features may be formed in different tectonic settings and involve components of both simple and pure shear. Shear zones may be classified into brittle, brittle-ductile or ductile-shear zones depending on the crustal depth level (Ramsay, 1980, Passchier and Trouw, 2005, Fossen and Cavalcante 2017, Meyer *et al.* 2017). Ductile deformation is dominated by crystal-plastic mechanisms (dislocation creep and twinning) and diffusion creep which produces rocks with foliation (mylonites) while brittle (or frictional) deformation is dominated by grain fracture, frictional sliding and grain rotation (Blenkinsop, 2000, Stipp *et al.*, 2002a,b, Vernon, 2004, Passchier and Trouw, 2005, Law, 2014). Within a shear zone, distinctive fabrics and mineral assemblages will indicate P-T conditions and the sense of motion for which the shear zone accommodates strain (Nicolas and Poirier, 1976, Vernon, 2004, Passchier and Trouw, 2005).

The Guaçuí and Batatal lineaments are two of the most strikingly geological features in the southern region of the Espírito Santo State (southeastern Brazil) and can be traced from satellite images and aerogeophysical data for tens to hundreds of kilometers. These lineaments developed in the final tectonic stages of the Neoproterozoic Araçuaí-West Congo orogen (Alkmim *et al.* 2006). In spite of its outstanding geographical expression, these geological features were studied only regionally and very few studies are available about its structural and deformational characteristics and metamorphic conditions (Silva, 2010). The study of shear zones usually involves petrographic and geological field descriptions coupled with geochronological and geochemical data (Passarelli *et al.* 2011, Phillips and Searle, 2007, Campanha 1981). In this sense, the aim of this study is to characterize and compare the geological and the structural features of the Guaçuí and Batatal lineaments. For this purpose, we integrated geological, macro- and microstructural data.

2. Geological and tectonic setting

The Araçuaí orogen, located in southeastern Brazil, and its African counterpart, the West Congo belt, constitute an orogenic system that developed during the Brasiliano-Pan-African orogeny between the margins of the São Francisco and Congo cratons (Figure 1, Alkmim *et al.*, 2006). The Araçuaí-West Congo orogenic system was formed during the amalgamation of Western Gondwana in Late Neoproterozoic time and split into two parts by opening of the South Atlantic Ocean in the Cretaceous. The Araçuaí orogen comprises rift-related to distal passive margin sequences, ophiolitic remnants of the precursor Macaúbas basin, Rio Doce magmatic arc-related rocks and collisional to post-collisional intrusions (Pedrosa Soares *et al.*, 2011). Pre-collisional magmatism (ca. 630-580 Ma) consists of I-type, metaluminous to slightly peraluminous, calc-alkaline granitoids (Tedeschi *et al.*, 2016). The arc-related supracrustal sequences is characterized by metavolcano-sedimentary successions of the Rio Doce group and metasedimentary sequences deposited in the fore-arc (Peixoto *et al.*, 2015) and back-arc (Gradim *et al.*, 2014) zones. Sin-collisional magmatism (ca. 585 – 545 Ma) mostly comprises S-type, peraluminous, sub-to calc-alkaline granitoids (Melo *et al.*, 2017). Post-collisional magmatism (ca. 525-480 Ma) includes of I-to A-types, metaluminous to slightly peraluminous, high K-Fe calc-alkaline to alkaline granites (Campos *et al.*, 2016, Pedrosa-Soares *et al.*, 2011). Paleoproterozoic to Archean basement rocks of the A-WC orogen include high-grade metamorphic rocks, such as granulites, intrusive charnockites and migmatites grouped into the Caparaó, Juiz de Fora, Ipanema, Guanhães and Serra do Valentim complexes. These represent reworked rocks related to the São Francisco Craton (Vieira *et al.* 2015, Alkmim *et al.* 2006).

The Araçuaí orogen is divided in nine structural domains developed in five tectonic stages according to Alkmim *et al.* (2006). The high-grade (crystalline) internal domain includes granite suites and paragneiss complexes, such as the Paraíba do Sul and Nova Venécia complexes (Figure 1). These are comprised of gneisses with intercalations of calc-silicate rocks, quartzites, amphibolites and marbles. The Paraíba do Sul Complex can be correlated to the Nova Venécia Complex, which is located in the northern region of the Espírito Santo State (Noce *et al.* 2004). The internal domain can be divided in two sub-domains. The southern subdomain contains a system of large-scale NNE-trending dextral transpressional shear zones that include the Guaçuí and Batatal shear zones (Cunninghan *et al.* 1998, Alkmim *et al.* 2006, Pedrosa-Soares *et al.* 2011). These shear zones were formed according to Vauchez *et al.* (1994) and Alkmim *et al.* (2006) as a response of the southward escape of the southern portion of the A-WC orogen and its extensional collapse at around 500 Ma.

The Guaçuí and Batatal shear zones are parallel structures about 80 km apart from each other (Figure 1). They cross para-derived gneisses belonging to the Paraíba do Sul/Jequitinhonha Complexes and pre to late-tectonic granitoids (Hasui, 2012, Pedrosa-Soares and Wiedmann-Leonardos, 2000, Silva, 1993). The Guaçuí Shear Zone (GSZ) is 350 km long and 5 km wide on average, and is comprised of mylonites and ultramylonites (core region), showing subvertical mylonitic foliation according to Silva (2010), Horn (2007) and Cunninghan *et al.* (1998). Silva (2010) estimated a horizontal displacement of 15 km for the GSZ and according to this author this structure was developed under medium to high-grade metamorphism. The Batatal Shear Zone (BSZ) is 70 km long and is comprised of mylonitic foliation, being interrupted to the south by the post-collisional Iconha pluton (Silva, 2010, Féboli, 1993). Silva (2010) estimated a horizontal displacement of 15 km for BSZ and according to this author, the BSZ would have originated under low to medium-grade metamorphism.

Vieira *et al.* (2015) presented a regional aeromagnetic geophysical survey for the state of Espírito Santo. The GSZ clearly lies on a large-scale linear geophysical anomaly. For BSZ, geophysical data anomalies occur in a discontinuous fashion way, just from the town of Marechal Floriano northwards.

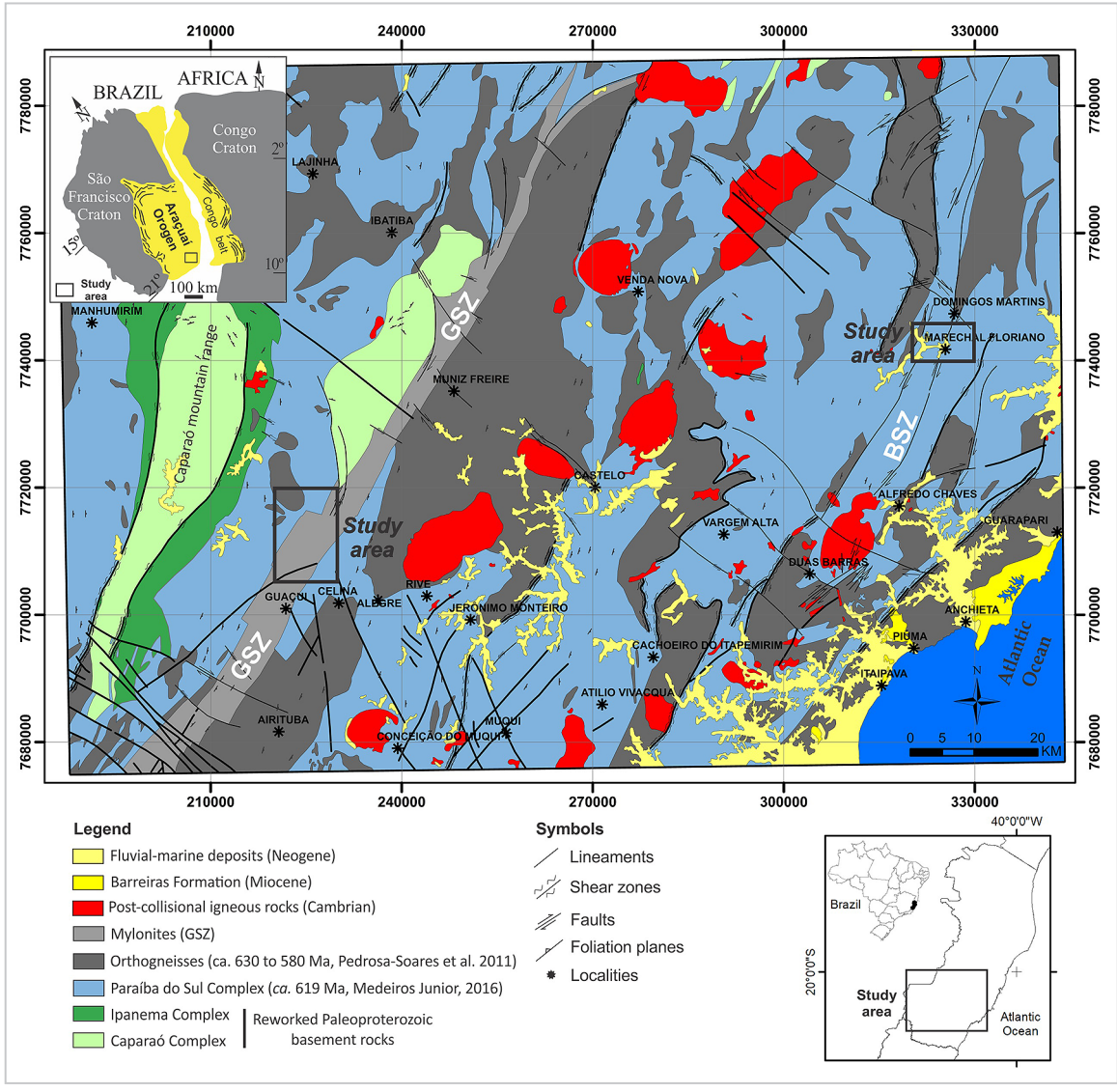

Figure 1 - Geological and tectonic framework of part of the southern region of the Espírito Santo State (southea stern Brazil) based on Vieira (1997) and Vieira et al. (2015). Legend: GSZ – Guaçuí Shear Zone and BSZ – Batatal Shear Zone.

3. Materials and Methods

The methodology involved the description of outcrops and collection of samples along profiles crosscutting both the GSZ and the BSZ. Cartographic data were georreferenced in ArcGIS 10.4 (ESRI, 2015) using the horizontal Datum WGS-84 and the UTM map projection (Zone 24S).

Fieldwork comprised the acquisition of geological and structural data and fresh rock samples for microstructural analysis. For the study of the GSZ, eight outcrops distributed in 16 km were described along the roads ES-185 and ES-387, between the district of Celina and the small town of Ibitirama (close to Guaçuí city, Figure 2). Nine thin sections were produced for this study. In addition, four thin sections (A3-05, A3-16, A4-308, A4-401) from other studies produced by the authors were included in the data set. For the study of the BSZ, 7 samples (1 oriented) distributed in 9.7 km were collected along the highway BR-262 in the region of the town of Marechal Floriano. All thin sections described hererin were cut in the X-Z structural plane. These samples were prepared in the Laboratory for Sample Preparation – LPA of the Federal University of the Espírito Santo – UFES/Campus Alegre and studied in a Nikon ECLIPSE E200 POL microscope. Petrographic, microstructural and field descriptions were based on Trouw *et al.* (2010), Paschier and Trouw (2005), Vernon (2004), Yardley (2004), Stipp *et al.* (2002a,b), Hirth and Tullis (1992) and Hobbs *et al.* (1976).

4. Results

4.1 Macrostructure of GSZ

Fieldwork reveled three main lithotypes. In outcrop 8, there occur metagranites and in outcrops 1, 2 and 7, orthogneisses. In all the other outcrops (3, 4, 5, 6, A03-05, A03-16, A04-308 and A04-401) mylonitic rocks are exposed (Figure 2). Besides, in one outcrop (UTM 24S 227154E/7713215S), a stromatic metatexite (migmatite gneiss) was also described very close to Point 4. It shows a subvertical and penetrative mylonitic foliation oriented parallel to the GSZ, transposed tight folds and dextral kinematic indicators (Figure 3).

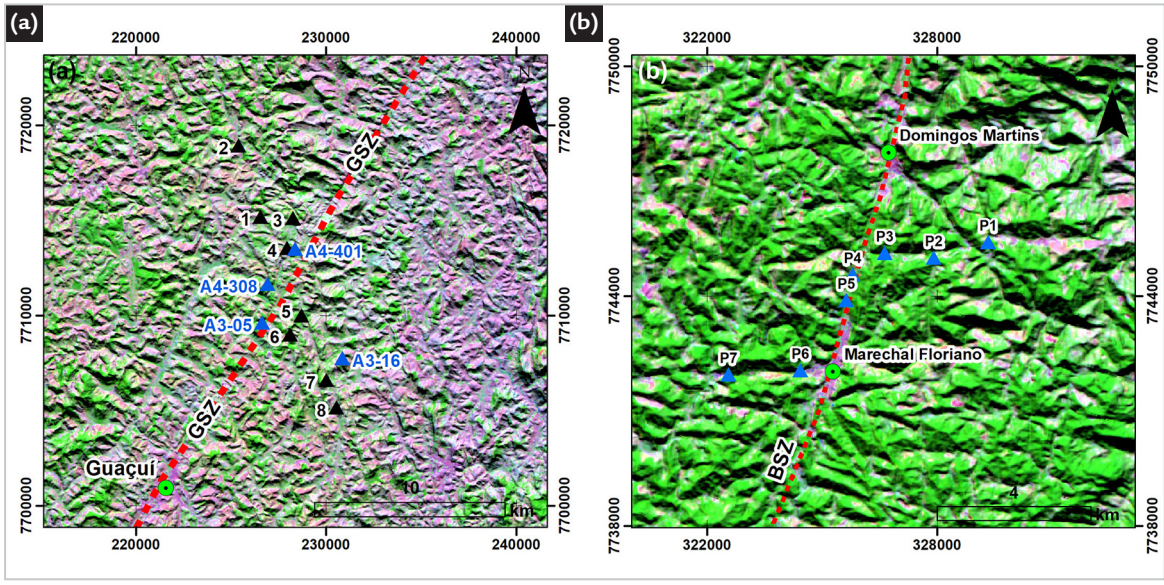

Figure 2 - Location of the studied outcrops: (a) GSZ and (b) BSZ. Blue triangles across the GSZ represent samples obtained from ancient fieldwork campaigns carried out by the authors.

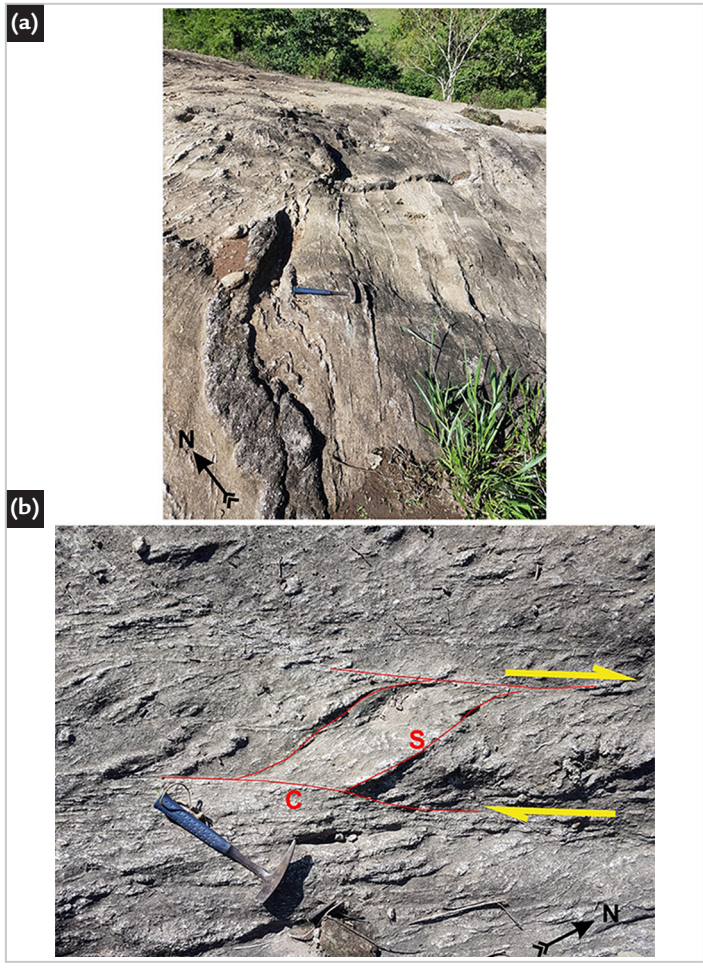

Figure 3 - Stromatic metatexite along GSZ (UTM 24S 227154E/7713215S): (a) Subvertical foliation oriented paralell to the GSZ (plain view) and (b) dextral kinematic indicator (plain view).

Metagranites are coarse-grained and leucocratic rocks, with weak discontinuous foliation defined by mm-sized biotite crystals. Orthogneisses are course to fine-grained rocks and show remarkable cm-sized gneissic banding. Deformed mafic enclaves, few decimeters in size, and sparingly migmatized zones are also observed. These rocks were associated to the Manhuaçú and Estrela orthogneisses (pre-collisional intrusions) (Horn, 2007). Mylonitic rocks show typical cm to mm-sized mylonitic banding and numerous ductile kinematic indicators, such as intrafoliar folds, asymmetric porphyroclasts, S-C foliation, etc. (Figure 4). These features, confirm the dextral shear sense described in other studies (Silva, 2010, Horn, 2007, Vieira, 1997). Subhorizontal NE to NNE-trending stretching lineations were also observed in few outcrops.

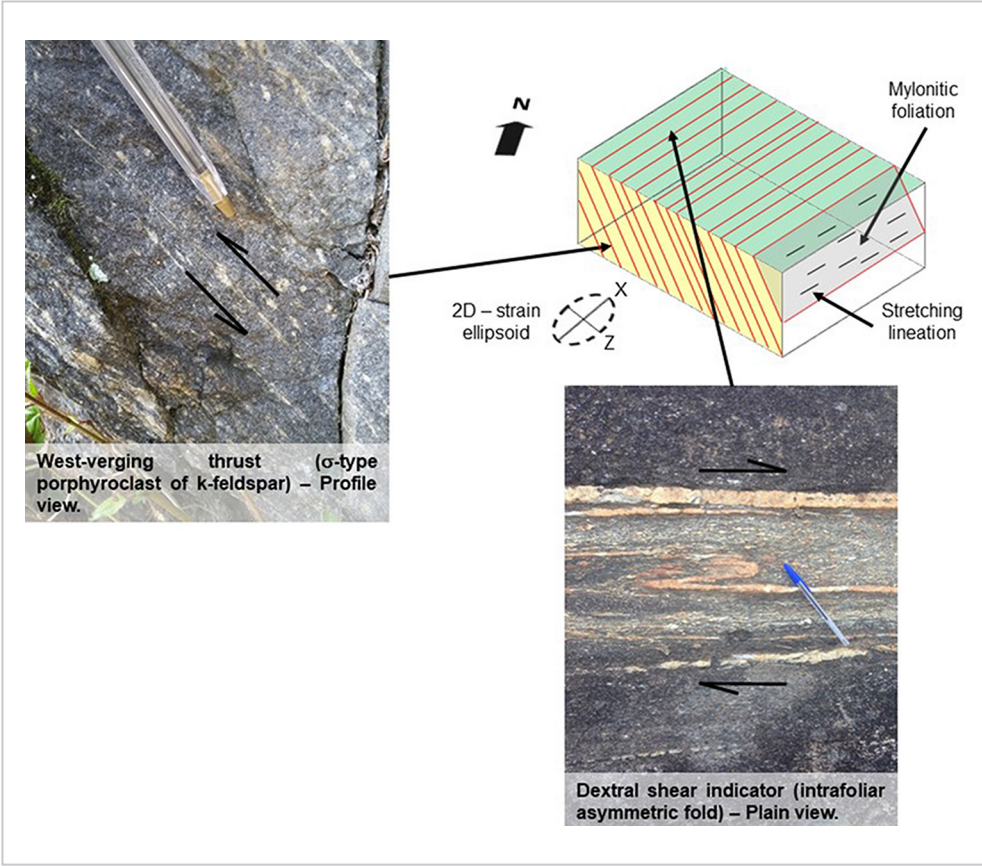

Figure 4 - Mylonitic rocks showing ductile kinematic indicators for the GSZ. Upper-left corner (outcrop 5) and bottom-right corner (outcrop 4).

Figure 5 depicts equal-area stereograms of all foliation planes measured along a NW-trending transect. As can be seen, foliation strike ranges from NNW to NNE with moderate to steep dip angles (45 - 64°) either to the east or to the west.

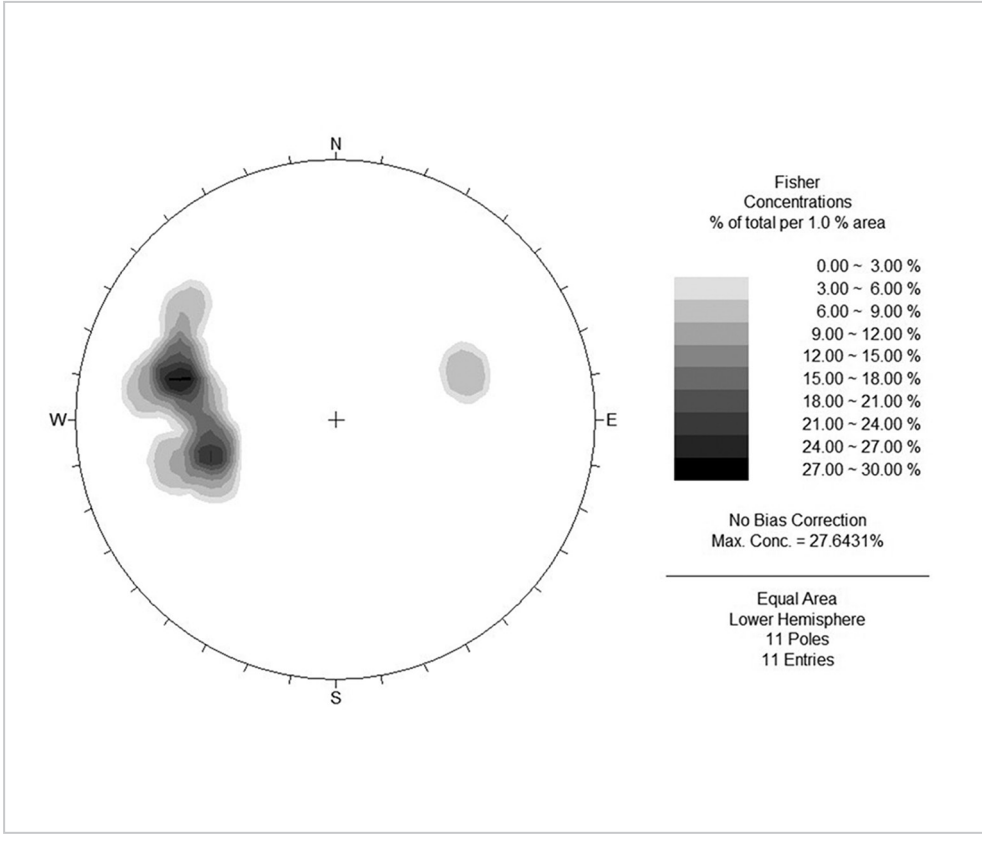

Figure 5 - Stereographic projection of planes of foliation across GSZ. Schmidt-Lambert net, lower hemisphere (equal area).

4.2 Microstructure of GSZ

Metagranites comprise incipient foliation, granoblastic texture, fine- to coarse-grained matrix with abundant subhedral feldspar crystals (Figure 6a). The mineral assemblage is characterized by plagioclase (12-33 vol.%), quartz (25-27 vol.%), K-feldspar (22-41 vol.%), biotite (8-15 vol.%) and magnetite (5-7 vol.%). Zircon and apatite dominate the accessory phases. Plagioclase (0.05-3.45 mm) occurs as subidioblastic to xenoblastic-fractured crystals that usually display undulose extinction and irregular polysynthetic twins. Some crystals show antiperthitic intergrowth of K-feldspar rods and rims partially replaced to muscovite. Quartz (0.05-3.65 mm) occurs as interstitial phase with polygonal to lobate grain boundaries. Some grains have undulose extinction and bulging of grain boundaries. Carlsbad twinning is a typical feature in subidioblastic K-feldspar crystals (0.09-6.33 mm), which can also show myrmekite intergrowth and triclinization processes (Figure 6a). Fractures are rare in K-feldspar grains. Biotite flakes (0.02-0.95 mm) are commonly associated to plagioclase and K-feldspar crystals and they can be slightly oriented. Some biotite rims have been partially altered to muscovite.

The orthogneisses show interlayered felsic and mafic foliated bands and monzogranitic to granodioritic compositons. The mineral assemblage is composed by quartz (27-39 vol.%), K-feldspar (6-14 vol.%), biotite (22-31 vol.%), plagioclase (8-19 vol.%), hornblende (4-11 vol.%) and rare garnet (~ 5 vol.%). Common accessory minerals are titanite, apatite, zircon and magnetite. The predominant texture is granolepidoblastic (Figure 6b) and subordinately nematoblastic. Quartz (0.02-3.70 mm) commonly presents undulose extinction and some crystals adopt a polygonal morphology with grain triple junction of approximately 120°. Some quartz grains contain numerous inclusions of apatite, zircon and biotite. Three textural varieties of biotite (0.03-1.83 mm) are recognized. The first type is characterized by inclusions in quartz, plagioclase and feldspar. Matrix biotite consists of small single crystals and/or clots of flakes aligned with the regional foliation. Zircon inclusions are common in these biotite crystals and some grains display rims that have been partially altered to magnetite. The last type occasionally occurs at the margins of the hornblende crystals. Plagioclase crystals (0.35-1.12 mm) show typical polysynthetic twinning and some crystals hosted apatite, zircon and biotite inclusions. Other features are irregular polysynthetic twinning boundaries, undulose extinction and occasionally intergrowth textures (e.g. antiperthite, myrmekite). Orthoclase occurs as xenoblastic grains, which commonly display Carlsbad twinning. In contrast to other orthogneiss samples, the AM-02-2 sample contains microcline grains in the felsic band. Lobate to polygonal contacts between quartz and feldspars are common features. Xenoblastic hornblende always occurs with lower modal abundance than biotite. Hornblende grains are frequently oriented and fractured. Garnet grains (~ 5 vol.%) exhibit rounded to hexagonal shapes (0.80-0.18 mm) that are frequently fractured. Alteration products of feldspars are characterized by sericite and carbonate formation.

Protomylonites are characterized by grain size reduction (<50% of the rock volume), where feldspar porphyroclasts, incipient S-C foliation and few kinematic indicators are observed. Fine-grained biotite and quartz wrap around feldspar porphyroclasts. Other microstructures observed are small aligned biotite flakes, which form disconnected trails along the grain boundaries of quartz. Mesomylonites display a well-defined planar fabric (C-foliation) and a mineral stretching lineation marked by the alignment of mica crystals and ribbon quartz. These rocks have a milimetric banding consisting of bands of different composition, hence with distinct rheologic properties. Mesomylonites consist of quartz, biotite, plagioclase, K-feldspar and occasionally hornblende and pyroxene. Accessory minerals are apatite, zircon and magnetite. The matrix is composed of oriented biotite aggregates and small quartz and feldspar grains. The most abundant porphyroclasts are feldspars and quartz. Minor constituents are hornblende and orthopyroxene. Quartz (25-53 vol.%) occurs both as large porphyroclasts (up to 10.5 mm), generally irregular grains with complex phase boundaries, and as finer (< 0.1 mm) grains in the matrix that have ameboid to sutured shapes (Figure 6c). Ribbons formed by polycrystalline quartz grains with undulose extinction are common. Other feature observed is triple junctions of approximately 120°. Plagioclase (8-27 vol.%) and orthoclase (7-20 vol.%) occur as non-fractured porphyroclasts (up to 5.8 mm), which are commonly surrounded by a mantle of fine-grained feldspar, and subordinately as recrystallized finer grains (0.01- 0.80 mm) in matrix. Some plagioclase grains display irregular polysynthetic twinning and σ-type shape. Undulose extinction, σ-type shape and *core mantle*-structures are features common in the orthoclase (Figure 6d,e). Other textures are occurrence of myrmekite along K-feldspar grain boundaries and perthite intergrowth. Aligned biotite flakes (10-28 vol.%) with sizes comprising between 0.04 and 0.93 mm define the foliation of the rock. Sigma-type hornblende porphyroclasts (5-15 vol.%) display recrystallized trails and some grains are fractured (Figure 6f). Normally, orthopyroxene (~ 4 vol.%) occurs as xenoblastic grains (0.07-0.80 mm) and in some cases exhibits strong elongate (ribbon texture with up to 2.03 mm) (Figure 6g). Magnetite (<4 vol.%) is commonly associated to biotite-rich bands. Apatite and zircon grains (< 1 vol.%) occur as fine-grained inclusions (0.03-0.46 mm) in quartz and orthoclase. Late reactions are common, and include local growth of white mica in feldspar and biotite. Ultramylonites (A3-05 and A4-401 samples) differ from mesomylonites primarily by a smaller, more uniform grain size (Figure 6h). Feldspar, amphibole, magnetite and biotite grains are fairly comminuted and recrystallized. The grains often exhibit amoeboid to sutured texture and some quartz ribbons are preserved. In these ultramylonite, the modal proportion of porphyroclasts and biotite decreases and compositional banding development increases.

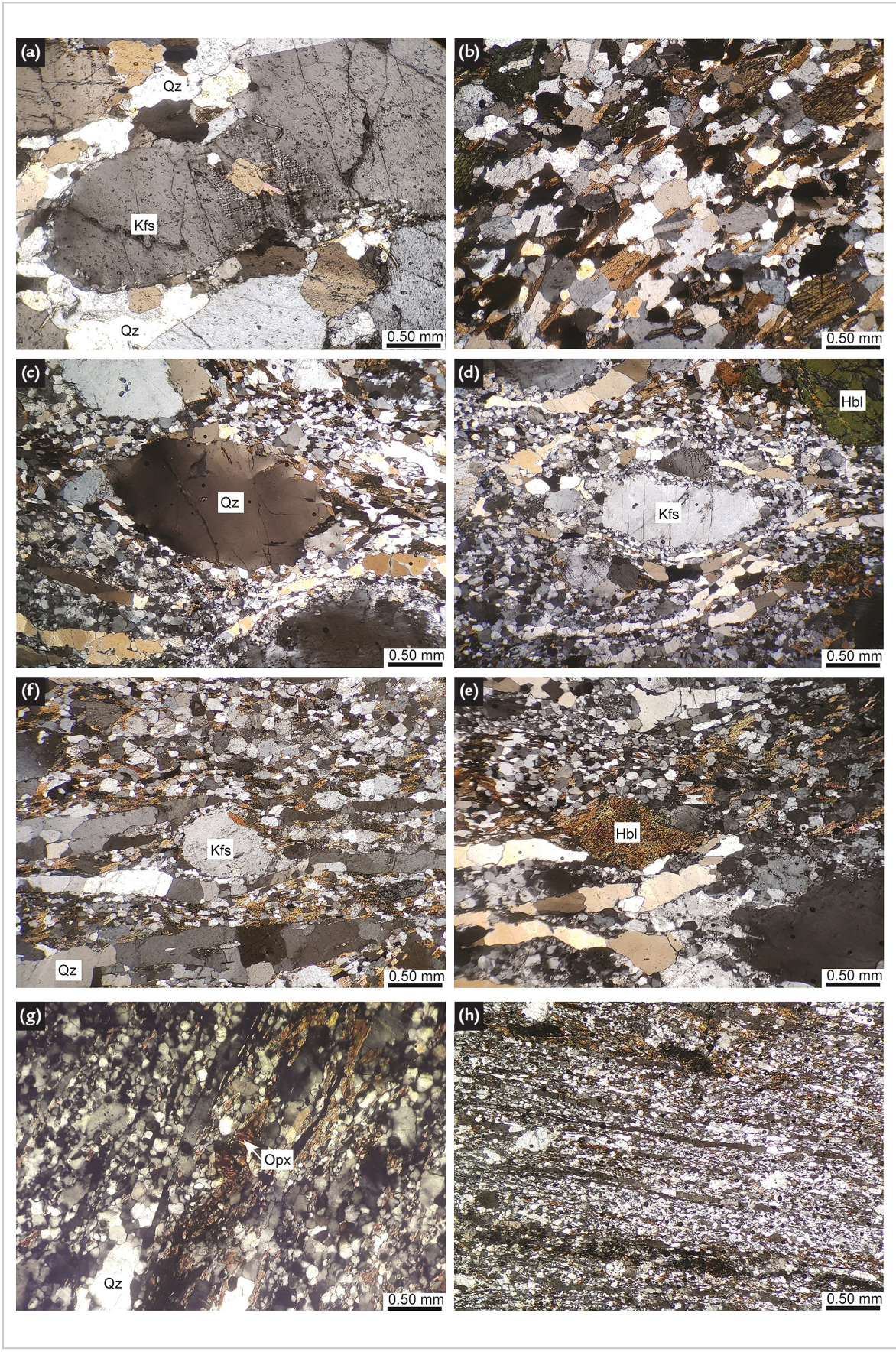

Figure 6 - Main microstructures observed in metagranites (a), orthogneisses (b) and mylonitic rocks (c to h) for the GSZ. (a) Partially triclinized-orthoclase showing lobate grain boundaries with quartz grains. (b) Granolepidoblastic texture showing biotite flakes oriented along the foliation (Sn). (c) Quartz porphyroclast with undulose extinction and mantled by recrystallized fine-grained grains. (d) Stretched feldspar crystal with core mantle-structure. (e) Quartz ribbons showing recrystallization evidence. Note the asymmetric shape indicated by K-feldspar porphyroclast. (f) Stretched hornblende crystal showing asymmetric recrystallized tails. (g) Recrystallized orthopyroxene grains tend to be stretched. (h) Extreme grain size reduction in ultramylonite.

4.3 BSZ Macrostructure

The transect course across the BSZ revealed a medium to coarse-grained garnet biotite gneiss (essentially deformed granodiorite to tonalite) (Figure 7a). Garnet crystals are reddish, varies from 0.2 to 1.5 cm in size, and present euhedral to subhedral habitus. Gneissic banding is made of alternating and parallel mafic and felsic banding. Banding thickness ranges from 0.1 to 3.0 cm in hand specimens. Mafic bands are essentially made of biotite and garnet crystals and acid bands are made of quartz, K-feldspar and plagioclase grains. A leucocratic garnet metatonalite was recognized in some outcrops (Figure 7b). Its foliation is characterized by undulose films of biotite flakes (< 1 mm in diameter on average). A fine-grained banded calcissilicatic rock was also identified (outcrop 3) (Figure 7c). Deformed mafic enclaves and sinistral kinematic indicators were observed in outcrop 6 (Figure 7d). In outcrop 2, there was also observed a medium-grained greyish green diorite dykes cutting garnet metatonalites.

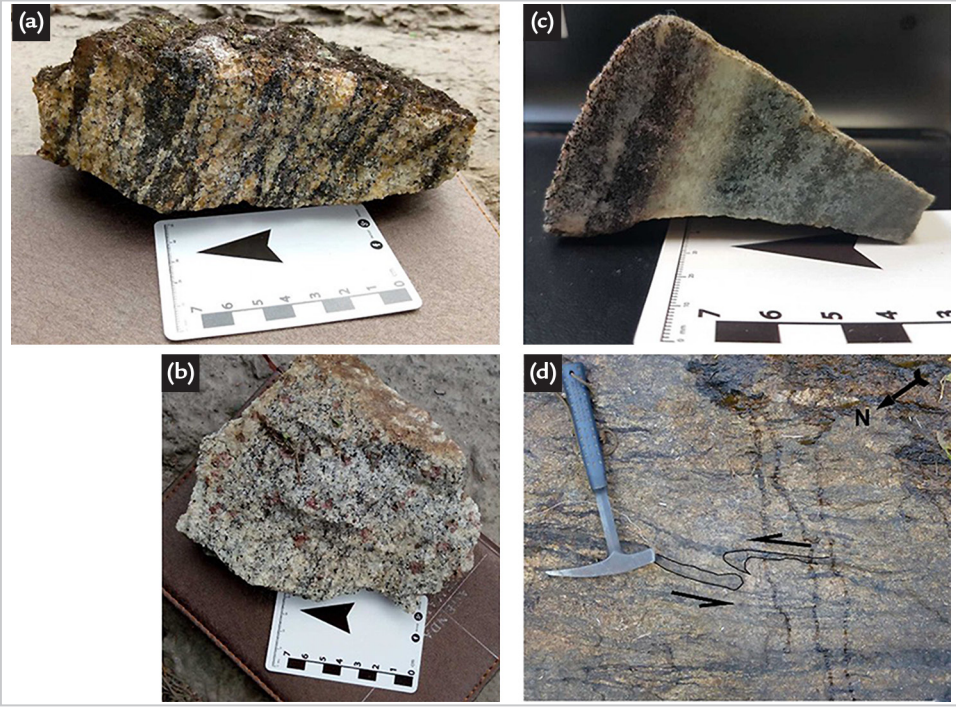

Figure 7 - Lithotypes and geological features observed for the BSZ: (a) orthogneiss showing a well-defined gneissic banding, (b) garnet metatonalite. Foliation can be seen as discontinuous undulose films of biotite flakes, (c) fine-grained calcissilicatic rock, and (d) sheared orthogneiss showing a sinistral kinematic indicator (plain view).

Figure 8 depicts stereograms of all foliation planes. Predominates NE to NNE-trending foliation with dip angles ranging from 10 to 88°. In outcrops 1, 2 and 3, a NW-trending foliation is observed with dip angles ranging from 20 to 60°. The significance of it is not clear, but could be associated to local parasitic folds. Due to the lack of cross-cutting evidence, relative chronology between both directions of foliation was not possible to be determined.

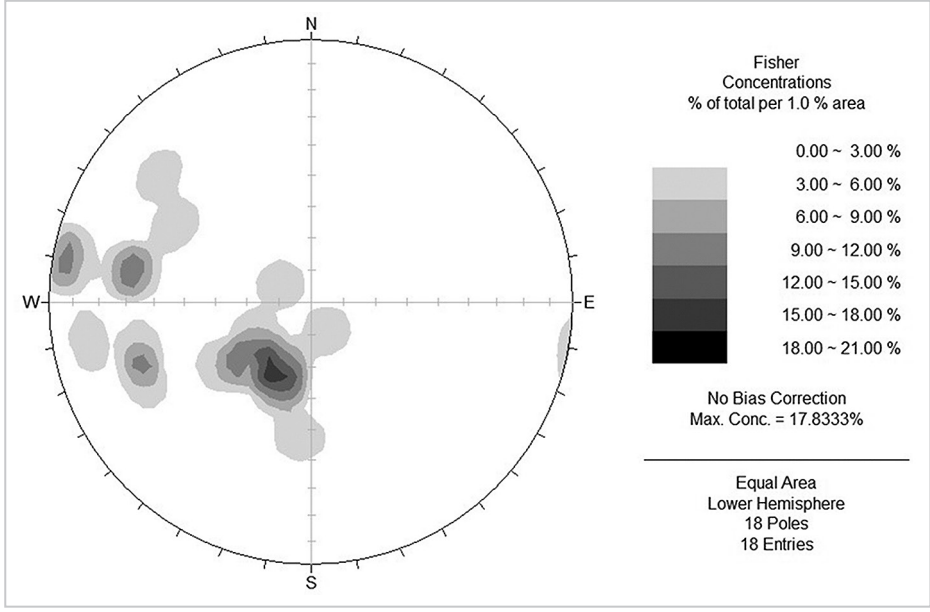

Figure 8 - Stereographic projection of foliation planes across BSZ. Schmidt-Lambert net, lower hemisphere (equal area).

4.4 BSZ Microstructure

The metatonalite and gneiss samples (P2, P4, P5 and P6) have a granolepidoblastic texture with polygonal and interlobate grain boundaries. Gneisses have mineralogical compositional similar to metatonalites, differing by sparce penetrative foliation. It consists of quartz (45-60 vol.%), plagioclase (10-25 vol.%), garnet (5-25 vol.%), biotite (15-20 vol.%), K-feldspar (5-10 vol.%) and traces (< 1vol.%) of apatite, zircon, ilmenite and secondary muscovite. In the gneiss, the thin biotite-garnet-rich mafic layers are commonly separated by very felsic layers composed by plagioclase, quartz and lesser amounts of K-feldspar. Quartz occurs as xenoblastic fine- to medium grained grains (0.10-4.5 mm), which occasionally hosted rounded biotite and zircon inclusions. Quartz grains show evidence of intracrystalline deformation (e.g., undulose extinction) and they are highly fractured in some samples (Figure 9a). Plagioclase (0.5-1.25 mm) occurs as xenoblastic and rarely as subidioblastic grains that shows polysynthetic twins according to albite and pericline laws. Plagioclase and quartz have interlobate to straight polygonal boundaries. The majority of plagioclase grains (P4, P5 and P6 samples) are cut by fissures (Figure 9a-b), which are filled with small mica. The main alteration product of plagioclase is white mica, mostly along cleavage planes and fractures. Biotite is the most common ferromagnesian mineral in these rocks.

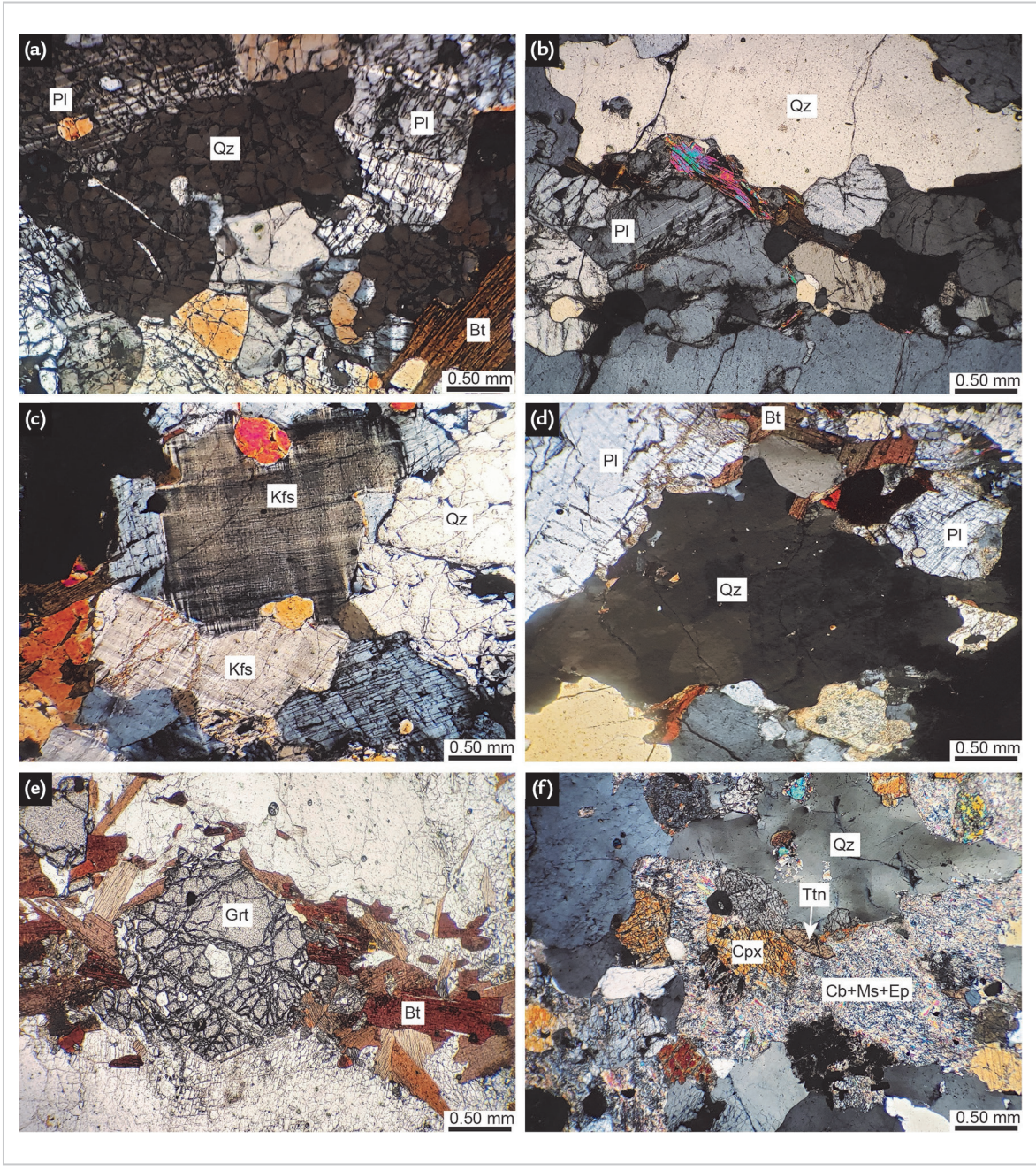

Figure 9 - Main microstructures observed in orthogneiss (a to c), paragneiss (d-e) and calcissilicatic rocks (f) for the BSZ. (a) Quartz and plagioclase grains highly fractured (P4 sample). (b) Plagioclase showing fractures filled by mica. Note that biotite and quartz are slightly fractured (P6 sample). (c) Microcline grains exhibit fractures occasionally filled by mica (P5 sample). (d) Quartz grain with undulose extinction in lobate contact with fractured plagioclase grains (P7 sample). (e) Fractured garnet porphyroblast with quartz and ilmenite inclusions (P7 sample). (f) Quartz with undulose extinction in carbonate-titanite-diopside-rich bands (P3 sample).

The mineral is commonly pale brown to reddish brown and contains zircon and quartz inclusion. Biotite occurs as rounded inclusions (< 0.1 mm) in garnet, flakes (0.25-4 mm) oriented parallel to the foliation and replacing garnet rims. The muscovite and ilmenite occurring in the border zone of biotite is their alteration product. Symplectic intergrowths of biotite and quartz were found in some samples (P2 and P6). Garnet poikiloblasts (0.25-3 mm) are idioblastic to subidioblastic and contain small inclusions of rounded biotite and lobate to rounded quartz. Garnet grains are extensively fractured, and the fractures are generally filled by biotite. K-feldspar (orthoclase or microcline) are xenoblastic (0.75-1.75 mm) and shows interlobate boundaries. Undulose extinction and fractures are common features (Figure 9c). Inclusions of quartz, biotite and plagioclase occur in large K-feldspar.

The inspection of P7 sample under microscope reveled a paragneiss composed by quartz (33 vol.%), K-feldspar (30 vol.%), biotite (15 vol.%), plagioclase (10 vol.%), garnet (10 vol.%) and minor sillimanite (2 vol.%). Apatite, zircon and ilmenite are accessory phases. Quartz (0.25-2.25) occurs as xenoblastic grains or as thin films at feldspar grains boundaries. Some grains show undulose extinction (Figure 9d). K-feldspar (0.50-4.75 mm) occurs as xenoblastic grains that may show embayed shapes and cuspate areas when surrounded by plagioclase, quartz and biotite. They are commonly perthitic and show fractures and undulose extinction. Biotite (0.1-1.5 mm) forms large single laths or clusters, generally with sillimanite and variably replacing garnet, and as smaller interstitial flakes. Biotite rims form symplectites with quartz in the proximity of garnet porphyroblasts. Xenoblastic plagioclase grains (0.50-1.5 mm) exhibit corroded rims and lobate inclusions of quartz. They locally show mirmekitic intergrowth and replacement by sericite along the fractures (Figure 9d). Subhedral garnet poikiloblasts (0.25-1.75 mm) contain lobate and rounded inclusions of quartz. Garnet grains are fractured (Figure 9e) and occasionally filled by biotite or ilmenite. Sillimanite (<0.25 mm) is idioblastic to subidioblastic and generally associated with biotite and garnet.

The calcissilicatic rock (P3 sample) is fine-to medium-grained with compositional layering defined by alternating garnet-biotite-plagioclase-quartz-rich layer (granolepidoblastic texture) and carbonate-diopside-titanite layers. It consists of quartz (40 vol%), diopside (15 vol%), plagioclase (10 vol%), biotite (10 vol%) and garnet (5 vol%). The accessory phases (1 vol%) are titanite, apatite, zircon and ilmenite. Carbonate, epidote and muscovite aggregates (19 vol%) are products of alteration. Quartz occurs as fine-to medium-grained xenoblastic grains (0.20-2.25mm) and occasionally presents an elongated shape (up to 3.75 mm). Undulatory extinction in quartz is most conspicuous in the elongated grains (Figure 9f). Fractures are often observed in xenoblastic to subidioblastic diopside grains (0.25-1.25 mm). Xenoblastic plagioclase (0.20-2 mm) shows the characteristic polysynthetic twinning and some grains are partially altered to white mica and carbonate in garnet-biotite-quartz-rich bands. Biotite (0.1-1 mm) is commonly oriented in the foliation, owing to mineral banding. It occurs associated to garnet-plagioclase-quartz-rich band. Poikiloblastic garnet (0.40-2.75 mm) is xenoblastic and contains numerous inclusions of rounded to lobate quartz and biotite (< 0.25 mm). Xenoblastic carbonate/muscovite/epidote aggregates are probably alteration product of plagioclase grains in titanite-diopside-rich bands (Figure 9f).

5. Discussion

The block diagrams presented in Figure 10 summarize the main geological and structural features described for both shear zones in the southern region of the state of Espírito Santo. Aligned landforms (ridges and valleys) are associated to both shear zones, extending tens of kilometers as reveled by satellite imagery.

Based on the meso- and microscopic structures, we interpret different deformation mechanisms associated with tectonics. Tectonic implications of geological structures are interesting topics and detailed studies of this aspect are very significant (e.g. Kaplay *et al*. 2016, Dasgupta and Mukherjee, 2017, Mukherjee *et al*. 2018).

The significant geological and microstructural differences between GSZ and BSZ reveal that they were developed at different crustal levels. Medeiros Júnior (2016) analyzed geothermobarometric data for calcissilicatic rocks exposed in the southern region of the state of the Espírito Santo (included in the Paraíba do Sul Complex), and obtained T = 690 to 790°C and P < 7 kbar, showing that rocks exposed in this region were indeed formed at great depths. Considering the level of crustal erosion of the exposed rocks of the southern region of the state of Espírito Santo, if both structures were coeval, mylonitic rocks metamorphosed under amphibolite facies conditions should be expected along BSZ. Thus, we interpret that BSZ must have developed in the very end stages of the tectonic collision of the Araçuaí Orogen and prior to the emplacement of post-collisional I-type granitoids, since the Iconha pluton interrupts BSZ alignment. Moreover, GSZ may have developed in the beginning of the lateral scape tectonic stage, soon after the emplacement of sin-collisional S-type granitoids.

GSZ is a typical ductile transpressive shear zone. Different rock types were affected by it, including metagranites, orthogneiss and sheared metatexites (pre-collisonal magmatism) and rocks metamorphosed in granulite facies (Archean to Paleoproterozoic basement rocks?). Dynamic deformation promoted extensive grain-size reduction in most of the studied samples (mylonitic rocks). Banding of the mylonitic rocks (GSZ) reflects flow partitioning during shearing, with strain in each individual band being accommodated by one or more specific deformation mechanism.

Vieira (1997) interpreted for the basement rocks of the Cachoeiro de Itapemirim Geological Sheet (1:250,000 scale) four deformation phases (Dn to D3). According to the author, deformation phase D1 produced NW to W thrusting and regional foliation while deformation phase D2, produced dextral shearing, including NNE-trending shear zones (e.g. Guaçuí Shear Zone). Ductile kinematic indicators found in mylonitic rocks of the GSZ indicate two senses of mass transport (Figure 4): i) NW thrusting and ii) NE dextral shearing. Horizontal NE-trending stretching lineations were recognized in very few outcrops. According to Tikoff and Greene (1997), pure shear-dominated transpression usually gives steep lineations (oblique) while simple shear-dominated transpression favors horizontal lineations. Therefore, we interpret GSZ as a simple shear-dominated transpression shear zone associated to progressive deformation.

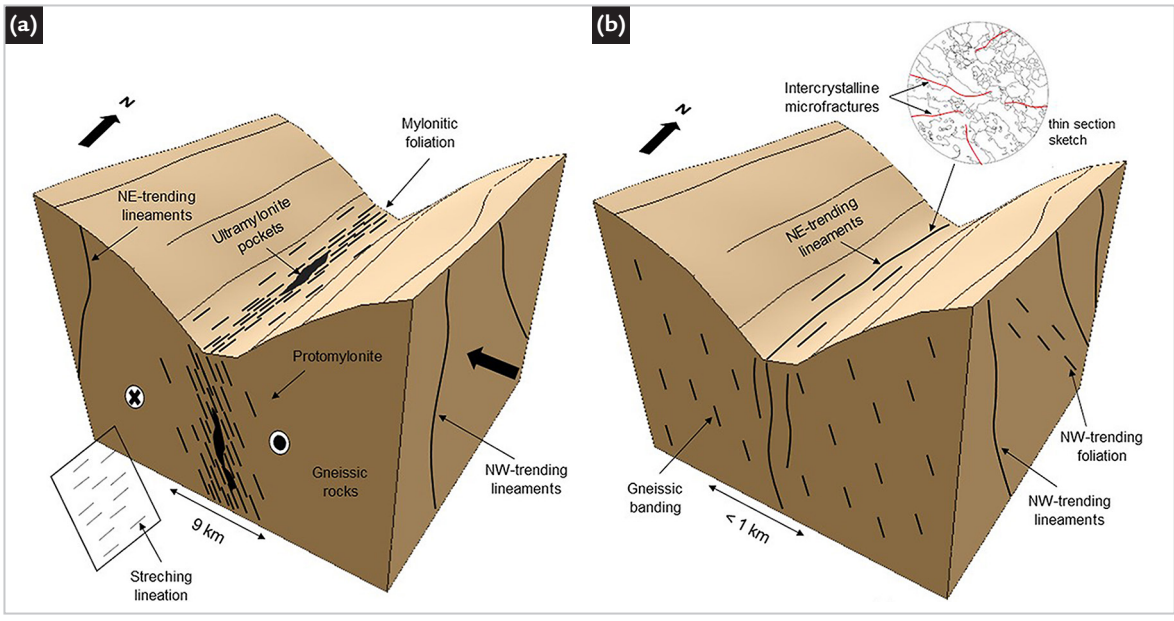

Figure 10 - Block diagrams illustrating the structural architecture of the GSZ (a)and the BSZ (b) for the southern region of the state of Espírito Santo.

Grain-scale features are consistent with the dextral shearing deformation revealed by S-C structures. Details of particle tracking in ideal faulted blocks using 3D co-ordinate geometry has been explained by Mukherjee (2019). Two main lines of evidence aid in determining deformation conditions for these rocks: (i) the quartz microstructures, and (ii) feldspar microstructures and textural relationships with other mineral phases. Quartz is the most ductile mineral phase, showing extensive dynamic recrystallization and ribbon development associated with large amounts of intracrystalline slip and grain boundary migration (Figure 6c to h). Undulose extinction in quartz porphyroclasts (Figure 6c) is caused by distortion of the crystal lattice by dislocations during intracrystalline plastic deformation (Blenkinsop, 2000). Amoeboid quartz grains were recrystallized under grain-boundary migration process. Microstructures in feldspar porphyroclasts also exhibit evidence for multiple phases of deformation. Plagioclase porphyroclasts commonly show undulose extinction due to intragranular dislocations, which is indicative of deformation by dislocation glide (Vernon, 2004, Passchier and Trouw, 2005). Another evidence of crystal plastic deformation is the presence of deformation twins in plagioclase. Grain-size reduction occurs through grain-boundary migration and/or subgrain rotation, producing a core-mantle structure (Figure 6d,e). The boundaries between adjacent feldspar grains are mainly ameboid, suggesting dynamic recrystallization through grain-boundary migration. A recrystallization process is accompanied by extensive grain-size reduction and locally by retrograde reactions involving the breaking down of feldspar and biotite into white mica.

ZCB is described as a brittle-ductile shear zone since ductile features like mylonitic foliation are superimposed by brittle features (Silva, 2010). Field observations and microstructural evidences have indicated the presence of orthogneisses and metatonalites with abundant garnet crystals (syn-collisonal intrusions?), and calcissilicatic rock and paragneiss (with garnet and sillimanite) (Paraíba do Sul Complex). A sheared orthogneiss showing sinistral kinematic indicator (outcrop 6) seems to predate the BSZ development (Figure 7). The foliation of these rocks is associated to the regional deformation phase (Vieira, 1997). In thin section, feldspar, quartz and garnet grains are generally deformed in a brittle manner, being transected by sets of intercrystalline microfractures (Figure 9). Microfracturing is observed throughout the study area. However, this process is more evidenced along the BSZ main trace. Interestingly, one of the samples (P4) exhibits microstructural features common to cataclastic rock in the upper lithosphere, such as: (i) primary grain shapes are preserved despite distinct generations of fracturing, and (ii) fracture sets do not show preferred orientation (Mitchell *et al*., 2011, Wechsler *et al*., 2011, Sullivan and Peterman, 2017).

Although GSZ and BSZ have been formed during the final tectonic stages of the Araçuaí-West Congo Orogen according to Alkmim *et al*. (2006) and Silva (2010), they originated under distinct deformational and metamorphic conditions according to our data. The microstructural data suggests that a mylonitization process reached greenschist to upper amphibolite facies conditions for GSZ. Mylonites show clear evidence of dynamic recrystallization of feldspar grains. Plagioclase is more indicative of temperature conditions, being recrystallized through subgrain rotation under medium to high temperature conditions (> 700° C). K-feldspar forms core-mantle structures (Figure 6d) under a larger range of temperatures between 400 and 650°C (Passchier and Trouw, 2005, Trouw *et al*., 2010). Subgrain rotation recrystallization of quartz and feldspar grains is expected to occur under temperatures > 400–500 °C, while grain-boundary migration may occur at > 500 °C (Law, 2014, Stipp *et al*., 2002b). Hornblende (Figure 6f) is more resistant to deformation than plagioclase and recrystallizes only at relatively high temperature (> 700 °C) in dry rocks (Passchier and Trouw, 2005). Recrystallized orthopyroxene (Figure 6g) is likely plastically deformed by high deformation temperature, which can reach up to 1000 °C (Passchier and Trouw, 2005, Trouw

et al., 2010).

In BSZ, the most outstanding microstructures are microfractures probably formed during the development of the shear zone. Microfracturing (Figure 9a-b) indicates that this process takes place at temperatures lower than 300°C (Pryer, 1993). The presence of intracrystalline deformation (e.g., undulose extinction) and lobate boundaries in some grains are evidence of deformation at low-grade conditions (Passchier and Trouw, 2005, Trouw *et al*., 2010) prior to BSZ development. The distinct microstructural features observed in both shear zones, indicate that they were formed under different pressure conditions.

6. Conclusions

The data presented in this study has indicated that GSZ is a dextral transpressive ductile shear zone that affected different lithotypes. Petrographic evidence indicates that GSZ does not represent a tectonic boundary separating distinct metamorphic terranes, since rocks observed in both sides are very similar in nature (Howell, 1995). Similar conclusions were found by Silva (2010). GSZ shows different levels of intensity of dynamic deformation, grading from protomylonites (outer margin) to ultramylonites (core region). Metamorphism may have reached upper amphibolite facies conditions. Ultramylonites occur as lenticular rock pockets enveloped by less strained rocks. Based on the distribution of the mylonitic-rocks, it is estimated that GSZ has an approximately 9 km width.

The lack of mylonites along BSZ, coupled with geological and petrographic evidence, have indicated that it is a narrow brittle shear zone. Its width cannot be accurately determined based on field observations and microstructure data, since all samples analyzed in this study record brittle microstructures (intercrystalline microfractures), indicating deformation at low-grade conditions. Based on the degree of mineral microfracturing of the analyzed rock samples, it is estimated that BSZ is less than 1 km wide in the region of the Marechal Floriano town.

The remarkable differences between GSZ and BSZ reveal that they were developed at different crustal levels. Although both are associated to the final stages of tectonic deformation of the Araçuaí-West Congo Orogen (late-collisional stage), our data indicate that GSZ must have developed prior to BSZ.

References

ALKMIM, F. F.; MARSHAK, S.; PEDROSA-SOARES, A. C.; PERES, G. G.; CRUZ, S. C. P.; WHITTINGON, A. Kinematic evolution of the Araçuaí-West Congo Orogen in Brazil and Africa: nutcracker tectonics during the Neoproterozoic assembly of Gondwana. ***Precambrian Research,*** v. 149, n. 1-2, p. 43-64, 2006.

BLENKINSOP, T. G. ***Deformation microstructures and mechanisms in minerals and rocks.*** Netherlands: Springer, 2000.

CAMPANHA, G. A. C. O Lineamento de Além Paraíba na área de Três Rios. ***Revista Brasileira de Geociências,*** v. 11, n.3, p. 159-171, 1981.

CAMPOS, C. P.; MEDEIROS, S. R.; MENDES, J. C.; PEDROSA-SOARES, A. C.; DUSSIN, I.; LUDKA, I. P.; DANTAS, E. L. Cambro-Ordovician magmatism in the Araçuaí Belt (SE Brazil): snapshots from a post-collisional event. ***Journal of South American Earth Sciences,*** v. 68, p. 248-268, 2016.

CUNNINGHAM, D.; ALKMIM, F. F.; MARSAKH, S. A structural transect across the coastal mobile belt in the Brazilian Highlands (latitude 20°S): the roots of a Precambrian transpressional orogen. ***Precambrian Research,*** v. 92, n. 3, p. 251-275, 1998.

DASGUPTA, S.; MUKHERJEE, S. Brittle shear tectonics in a narrow continental rift: asymmetric nonvolvanic Barmer Basin (Rajasthan, India). ***Journal of Geology,*** v. 125, n. 5, p. 561-591, 2017.

ESRI. ***ArcGIS Desktop***: Release 10.4. Redlands, CA: Environmental Systems 498 Research Institute, 2015.

FÉBOLI, W. L. (org.). ***Domingos Martins – Folha SF.24-V-A-III***: Estado do Espírito Santo, texto explicativo e carta geológica. Escala 1:100.000. Brasilia: DNPM/CPRM, 1993. 179 p. (Programa Levantamentos Geológicos Básicos do Brasil).

FOSSEN, H.; CAVALCANTE, G. C. Shear zones: a review. ***Earth-Science Reviews,*** v. 171. p. 434–455, 2017.

GRADIM, C.; RONCATO, J.; PEDROSA-SOARES, A.C.; CORDANI, U.; DUSSIN, I.; ALKMIM, F. F.; QUEIROGA, G.; JACOBSSOHN, T.; SILVA, L. C.; BABINSKI, M. The hot back-arc zone of the Araçuaí orogen, Eastern Brazil: from sedimentation to granite generation. ***Brazilian Journal of Geology.*** v. 44, n. 1, p. 155–180, 2014

HAMSAY, J. G. Shear zone geometry: a review. ***Journal of structural geology,*** v. 2, n. 1-2, p. 83-99, 1980.

HASUI, Y. Sistema Orogênico Mantiqueira. *In*: HASUI, Y.; CARNEIRO, C. D. R.; ALMEIDA, F. F. M.; BARTORELLI, A. ***Geologia do Brasil.*** São Paulo: Becca, 2012.

HIRTH, G.; TULLIS, J. Dislocation creep regimes in quartz aggregates. ***Journal of Structural Geology,*** v. 14, n. 2, p. 145-159, 1992.

HOBBS, B. E.; MEANS, W. D.; WILLIAMS, P. F. ***An outline of structural geology.*** New York: Wiley, 1976. 571 p.

HOWELL, D. G. ***Principles of terrane analysis***: new applications for global tectonics. 2nd. ed. New York: Chapman and Hall, 1995. 264 p.

HORN, A. H. ***Programa geologia do Brasil - Levantamentos geológicos básicos***: geologia da Folha Espera Feliz - SF.24-V-A-IV. Escala 1:100.000. Brasília: CPRM, 2007. 63 p.

INSTITUTO BRASILEIRO DE GEOGRAFIA E ESTATÍSTICA. ***Folha topográfica Domingos Martins***: Folha SF-24-V-A-III-4. Rio de Janeiro: IBGE, 1978. Escala 1:50.000.

INSTITUTO BRASILEIRO DE GEOGRAFIA E ESTATÍSTICA. ***Folha topográfica Divino de São Lourenço***: Folha SF-24-V-A-IV-2. Rio de Janeiro: IBGE, 1977. Escala 1:50.000.

KAPLAY, R. D.; SHAIKH, M. B.; MUKHERJEE, S.; VIJAY KUMAR, T. Morphotectonic expression of geological structures in the eastern part of the South East Deccan Volcanic Province (around Nanded, Maharashtra, India). *In*: MUKHERJEE, S.; MISRA, A. A.; CALVÈS, G.; NEMČOK, M. ***Tectonics of the Deccan large igneous province***. London: Geological Society London, 2016. (Geological Society London Special Publications, v. 445). DOI 10.1144/SP445.12.

LAW, R. D.; SCHMID, S. M.; WHEELER, J. Simple shear deformation and quartz crystallographic fabrics: a possible natural example from the Torridon area of NW Scotland. ***Journal of Structural Geology.*** v. 12, n. 1, p. 29 – 45, 1990.

MEDEIROS JÚNIOR, E. B. ***Evolução petrogenética de terrenos granulíticos nos estados de Minas Gerais e Espírito Santo.*** 2016. 167 f. Tese (Doutorado em Evolução Crustal e Recursos Naturais) - Escola de Minas, Universidade Federal de Ouro Preto, Ouro Preto, 2016.

MELO, M. G.; STEVENS, G.; LANA, C.; PEDROSA-SOARES, A. C.; FREI, D.; ALKMIM, F. F.; ALKMIN, L. A. Two cryptic anatectic events within a syn-collisional granitoid from the Araçuaí orogen (southeastern Brazil): evidence from the polymetamorphic Carlos Chagas batholith. ***Lithos,*** v. 277. p. 51-71, 2017.

MEYER, S. E.; KAUS, B. J. P.; PASSCHIER C. Development of branching brittle and ductile shear zones: a numerical study. ***Geochemistry, Geophysics, Geosystems,*** v. 18, n. 6, p. 2054–2075, 2017.

MITCHELL, T. M.; BEN-ZION, Y.; SHIMAMOTO T. Pulverized fault rocks and damage zone asymmetry along the Arima-Takatsuki Tectonic Line, Japan. ***Earth and Planetary Science Letters,*** v. 308, n. 3-4, p. 284-297, Aug. 2011.

MUKHERJEE, S. Particle tracking in ideal faulted blocks using 3D co-ordinate geometry. ***Marine and Petroleum Geology,*** v. 107, p. 508-514, Sep. 2019. DOI 10.1016/j.marpetgeo.2019.05.037.

MUKHERJEE, S.; GOSWAMI, S.; MUKHERJEE, A. Structures and their tectonic implications of the southern part of the Cuddapah Basin, Andhra Pradesh, India. ***Iranian Journal of Science and Technology,*** v. 43, n.2, 2018. DOI 10.1007/s440995-018-0566-0.

NICOLAS, A.; POIRIER, J. P. ***Crystalline plasticity and solid-state flow in metamorphic rocks.*** London: John Wiley and Sons, 1976. 444 p.

NOCE, C. M.; PEDROSA-SOARES, A. C.; PIUZANA, D.; ARMSTRONG, R.; LAUX, J. H.; CAMPOS, C. M.; MEDEIROS, S. R. Ages of sedimentation of the kinzigitic Complex and of a late orogenic termal episode in the Araçuaí orogen, northern Espírito Santo State, Brazil: zircon and monazite U-Pb SHRIMP and ID-TIMS data. ***Revista Brasileira de Geociências.*** v. 34, n. 4, p.587-592, 2004.

PASSARELLI, C. R.; BASEI, M. A. S.; WEMMER, K.; SIGA, O.; OYHANTÇABAL, P. Major shear zones of southern Brazil and Uruguay: escape tectonics in the eastern border of Rio de La plata and Paranapanema cratons during the Western Gondwana amalgamation. ***International Journal of Earth Sciences,*** v. 100, n. 2-3, p. 391-414, 2011. DOI: https://doi.org/10.1007/s00531-010-0594-2.

PASSCHIER, C. W.; TROUW, R. A. J. ***Microtectonics.*** Berlin: Springer-Verlag, 2005.

PEDROSA-SOARES, A. C.; DE CAMPOS, C. P.; NOCE, C.; SILVA, L. C.; NOVO, T.; RONCATO, J.; MEDEIROS, S.; CASTAÑEDA, C.; QUEIROGA, G.; DANTAS, E.; DUSSIN, I.; ALKMIM, F. Late Neoproterozoic–Cambrian granitic magmatism in the Araçuaí orogen (Brazil), the Eastern Brazilian Pegmatite Province and related mineral resources. *In*: SIAL, A. N.; BETTENCOURT, J. S.; CAMPOS, C. P.; FERREIRA, V. P. ***Granite-related ore deposits.*** London: Geological Society London, 2011. p. 25-51. (Geological Society London Special Publications, v. 350).

PEDROSA-SOARES, A. C.; WIEDMANN-LEONARDOS, C. M. Evolution of the Araçuaí Belt and its connection to the Ribeira Belt, Eastern Brazil. *In*: CORDANI, U.; MILANI, E. J.; THOMAZ, A.; CAMPOS, D. A. (ed.). ***Tectonic evolution of South America***. Rio de Janeiro: SBG, 2000. p. 265-285.

PEIXOTO, E.; PEDROSA-SOARES, A. C.; ALKMIM, F. F.; DUSSIN, I. A. A suture-related accretionary wedge formed in the Neoproterozoic Araçuaí orogen (SE Brazil) during Western Gondwanaland assembly. ***Gondwana Research,*** v. 27, n. 2, p. 878–896, 2015.

PHILLIPS, R. J.; SEARLE, M. P. Macrostructural and microstructural architecture of the Karakoram fault: relationship between magmatismo and strike-slip faulting. ***Tectonics,*** v. 26, TC3017, 2007. DOI 10.1029/2006TC001946.

PRYER, L. L. Microstructures in feldspars from a major crustal thrust zone: the Grenville Front, Ontario, Canada. ***Journal of Structural Geology,*** v. 15, n. 1, p. 21-36, 1993.

RAMSAY, J. G. Shear zone geometry: a review. ***Journal of Structural Geology,*** v. 2, n. 1-2, p. 83–99, 1980.

SILVA, C. M. T. ***O sistema transcorrente da porção sudeste do orógeno Araçuaí e norte da faixa Ribeira***: geometria e significado tectônico. 2010. 221 f. Tese (Doutorado em Evolução Crustal e Recursos Naturais) - Escola de Minas, Universidade Federal de Ouro Preto, Ouro Preto, 2010.

STIPP, M.; STUNITZ, H.; HEILBRONNER, R.; SCHMID, S. Dynamic recrystallization of quartz: correlation between natural and experimental conditions. *In*: MEER, S.; DRURY, M. R.; BRESSER, J. H. P.; PENNOCK, G. M. (ed.). ***Deformation mechanisms, rheology and tectonics***: current status and future perspectives. London: Geological Society London, 2002a. p. 171-190. (Geological Society London Special Publications, v. 200).

STIPP, M.; STUNITZ, H.; HEILBRONNER, R.; SCHMID, S. The eastern Tonale fault zone: a natural laboratory for

crystal plastic deformation of quartz over a temperature range from 250 to 700°C. ***Journal of Structural Geology,*** v. 24, n. 12, p. 1861-1884, 2002b.

SULLIVAN, W. A.; PETERMAN, E. M. Pulverized granite at the brittle-ductile transition: An example from the Kellyland fault zone, eastern Maine, U.S.A. ***Journal of Structural Geology,*** v.101, p. 109-123, 2017.

TEDESCHI, M.; NOVO, T.; PEDROSA-SOARES, A. C.; DUSSIN, I.; TASSINARI, C.; SILVA, L. C.; GONÇALVES, L.; ALKMIM, F.; LANA, C.; FIGUEIREDO, C.; DANTAS, E.; MEDEIROS, S.; CAMPOS, C.; CORRALES, F.; HEIBRON, M. The Ediacaran Rio Doce magmatic arc revisited (Araçuaí-Ribeira orogenic system, SE Brazil). ***Journal of South American Earth Sciences,*** v.68, p. 248–268, 2016.

TIKOFF, B.; GREENE, D. Stretching lineations in transpressional shear zones: an example from the Sierra Nevada Batholith. ***Journal of Structural Geology,*** v. 19, n. 1, p. 29-39, 1997.

TROUW, R. A. J.; PASSCHIER, C. W.; WIERSMA, D. J. ***Atlas of mylonites***: and related microstructure. Heidelberg: Springer, 2010.

VAUCHEZ, A.; TOMMASI, A.; EGYDIO-SILVA, M. Self-indentation of a heterogeneous continental lithosphere. ***Geology,*** v. 22, n. 11, p. 967–970, 1994.

VERNON, R. H. ***A practical guide to rock microstructure.*** Cambridge: Cambridge University Press, 2004.

VIEIRA, V. S.; SILVA, M. A.; CORREA, T. R.; LOPES, N. H. B. (org.) ***Geologia e recursos minerais do Estado do Espírito Santo***: mapas geológicos estaduais. Escala 1:400.000. Belo Horizonte: CPRM: Serviço Geológico do Brasil, 2015. 289 p. (Programa Geologia do Brasil, Coleção Mapas Geológicos Estaduais).

VIEIRA, V. S. (org.). ***Cachoeiro do Itapemirim – Folha SF.24-V-A***: Estados do Espírito Santo, Minas Gerais e Rio de Janeiro. Escala 1:250.000. Brasília: CPRM, 1997. 99 p. (Programa Levantamentos Geológicos Básicos do Brasil).

YARDLEY, B. W. D. Introdução à petrologia metamórfica. 2. ed. Brasília: Editora Universidade de Brasília, 2004.

WECHSLER, N.; ALLEN, E. E.; ROCKWELL, T. K.; GIRTY, G.; CHESTER, J. S.; BEN-ZION, Y. Characterization of pulverized granitoids in a shallow core along the San Andreas fault, little rock CA. ***Geophysical Journal International,*** v.186, n. 2, p. 401-417, 2011.

Received: 30 March 2020 - Accepted: 16 July 2020.